Simultaneous regularization method for the determination of radius distributions from experimental multiangle correlation functions

R. Buttgereit,* T. Roths, and J. Honerkamp
Albert-Ludwigs-Universität, Freiburger Materialforschungszentrum Stefan-Meier-Strasse 21, D-79104 Freiburg im Breisgau, Germany

L. B. Aberle †
Fraunhofer Institut für Fertigungstechnik und Angewandte Materialforschung, Wiener Strasse 12, 28359 Bremen, Germany
(Received 11 January 2001; published 24 September 2001)

Dynamic light scattering experiments have become a powerful tool in order to investigate the dynamical properties of complex fluids. In many applications in both soft matter research and industry so-called ''real world'' systems are subject of great interest. Here, the dilution of the investigated system often cannot be changed without getting measurement artifacts, so that one often has to deal with highly concentrated and turbid media. The investigation of such systems requires techniques that suppress the influence of multiple scattering, e.g., cross correlation techniques. However, measurements at turbid as well as highly diluted media lead to data with low signal-to-noise ratio, which complicates data analysis and leads to unreliable results. In this article a *multiangle regularization method* is discussed, which copes with the difficulties arising from such samples and enhances enormously the quality of the estimated solution. In order to demonstrate the efficiency of this multiangle regularization method we applied it to cross correlation functions measured at highly turbid samples.

DOI: 10.1103/PhysRevE.64.041404 PACS number(s): 82.70.−y, 02.30.Zz, 05.40.−a, 82.80.Dx

I. INTRODUCTION

Dynamic light scattering (DLS) experiments have become a powerful tool in order to investigate the dynamical properties of complex fluids, e.g., through the diffusion constants or the hydrodynamic *radius distribution* of soluted particles. These distributions have to be inferred from measured correlation functions of the scattered light by inverting a nonlinear integral equation. This is known to be an *ill-posed inverse problem*, since the distribution does not depend continuously upon the data [1,2]. Accordingly, small aberrations in the experimental data, which are inevitably effected by measurement errors, will result in large or even unbounded errors of the reconstructed distribution. Thus, one might say that the data do not contain the whole information in order to reconstruct properly the distribution. Accordingly, in order to solve such ill-posed problems so-called regularization methods are necessary corresponding to maximum a posteriori (MAP) estimators, [3–6]. These methods impose some prior information on the solution in order to compensate the ''lack of information'' in the data due to the measurement errors.

The inversion of an ill-posed problem becomes complicated for low signal-to-noise ratios and for small numbers of data points, i.e., for a small amount of data information. In the case of DLS data the error is mainly given by an estimation error of the hardware correlator, which is used in order to estimate the correlation of the detected photons. This data error increases with decreasing number of singly scattered photons, which may be due to multiple scattering processes in the case of turbid media or due to a small number of scattering processes in the case of highly diluted media. Therefore, especially in such cases of low signal-to-noise ratio (or if a high resolution is desired [7]), common regularization methods based on the data of only *one* scattering angle are not able to resolve properly the distribution.

However, this problem can be overcome by using the maximum data information obtained from the experiment. Therefore, all measured data of all scattering angles have to be taken into account. The simultaneous analysis of all data from all scattering angles takes advantage of three important points.

(1) Much more data—and thus much more information—is used for the inversion of the ill-posed problem.

(2) The scattering characteristics of the soluted particles vary for different scattering angles. Thus—in dependence on the measurement angle—specific particle sizes contribute less to the entire scattering intensity. Accordingly, these particle sizes are worse resolvable using a single angle analysis. Simultaneous multiangle regularization method, however, compensates these lower information in *one* correlation function by the correlation functions of *the other* measurement angles. Thus, all particle sizes can be resolved quite equally.

These two points lead to a ''better conditioning'' of the inverse problem as discussed in [8]. Thus, in case of high signal-to-noise ratio simple inversion methods such as ''multiangle'' non-negative least squares or singular value analysis may succeed [9,10]. However, these methods, which are based entirely on the data information but do not impose any prior information on the solution, break down for data with a low signal-to-noise ratio as discussed in this article. Furthermore, in addition to these common advantages of multiangle analysis, a third advantage has to be regarded.

(3) A separate analysis of correlation functions for each

*Email address: buttgere@fmf.uni-freiburg.de
†Email address: ab@ifam.fhg.de

scattering angle leads to a couple of estimates of the desired size distribution. Each of them satisfies the prior information, e.g., that the distribution is smooth, but not necessarily their combination, i.e., their weighted mean. Thus, the prior information is not defined consistently. However, the simultaneous analysis of all data leads to *one* consistent estimate, which satisfies properly the prior information.

In this paper we demonstrate the efficiency of this modified MAP estimator, in the following called multiangle MAP (maMAP) estimator. Therefore, it is compared with the commonly used single angle MAP (saMAP) estimator by applying both saMAP and maMAP to cross correlation functions measured with rather *turbid samples*.

These so-called ''real world'' samples, which are of great interest in both soft condensed matter research and industry, often cannot be investigated by conventional DLS. This is due to the fact that turbid media in general lead to significant amounts of multiple scattering that results in unreliable and erroneous evaluation of the data.

In order to overcome this problem in the last decade a number of different measurement schemes based on cross correlation techniques have been developed and it has been demonstrated that these techniques are powerful tools for an effective suppression of the disturbing influence of multiply scattered light in turbid media [11–18].

The measurements presented in this article were performed with the three-dimensional (3D) cross correlation technique [19–21], which is a very handy method for angle dependent measurements. With cross correlation experiments the error is due to two different reasons: On the one hand the signal-to-noise ratio of measured cross correlation functions strongly depends on the alignment of the optical elements, which is highly pretentious. This experimental disadvantage is counterbalanced by the fact that no systematic errors due to multiple scattering occur. On the other hand for very strongly scattering samples the fraction of singly scattered light become very small due to an overwhelming amount of multiple scattering processes. Thus the statistical accuracy of cross correlation experiments decreases. As known from conventional light scattering experiments with nearly transparent samples, noise on the experimental data can lead to broadened size distributions and unreproducible peak positions. Therefore, it has been a challenge to code a multiangle evaluation scheme that keeps pace with the experimental developments for investigation of turbid samples and optimize the evaluation of experimental data by multiangle data analysis.

This article is structured in the following way: After the presentation of the multiangle regularization procedure it is applied to data of cross correlation functions obtained with turbid samples containing monomodal latex particles. It is shown that the maMAP estimator indeed enhances enormously the quality of the calculated radical distributions. Furthermore, maMAP leads to *one* consistent estimate of the radius distribution for all data with a proper reconstruction of the distribution shape, which is close to reality.

We go further and analyze cross correlation functions obtained with samples containing two types of spherical particles that have fairly well defined and rather similar particle sizes but much different volume fractions. In such cases evaluation of correlation functions is considered as highly problematic and inverse Laplace procedures require correlation functions of high quality and with a high signal-to-noise ratio. Otherwise, deviations of the resulting correlation functions from a simple exponential can hardly be recognized, not to mention be evaluated. In order to enhance the resolution one has to perform measurements for different scattering angles [9,22]. However, the results of the Laplace inversion techniques are still sensitive to noise on the experimental data. We demonstrate that our multiangle regularization method as proposed in [6,7] copes with the difficulties arising from such samples and yields correct radius distributions.

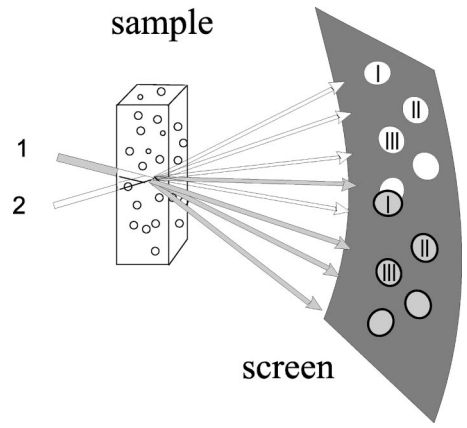

FIG. 1. Schematic sketch of the 3D principle. Two scattering experiments, (1) and (2), are tilted against each other in such a way that the two scattering vectors and scattering volumes are the same, but the corresponding wave vectors do not coincide. On a screen in the far field the two laser beams give rise to two speckle patterns that are also shifted with respect to each other. The signals of detectors placed at the positions of equivalent speckles (marked by identical numbers) are correlated. A more detailed description is given in the text.

II. 3D CROSS CORRELATION METHOD

The performance of the 3D cross correlation apparatus is described in detail in [20]. Therefore, in this paper we restrict the description to the basic ideas of the method and of the setup. The 3D cross correlation technique takes advantage of the fact that the properties of singly scattered light depend in a unique way on the scattering vector **q**, which is given by the difference of the initial and final wave vector. The idea is to perform simultaneously two scattering experiments in a three-dimensional geometry in such a way that the two *scattering vectors* and *scattering volumes* are the same, but the corresponding *wave vectors* do not coincide.

Figure 1 shows a sketch explaining of this idea in a somewhat oversimplified way. Here, the sample is illuminated by two laser beams tilted against each other by an angle of ϕ. On a screen in the far field these two laser beams give rise to two speckle patterns that are also shifted with respect to each other according to ϕ. It is then obvious that the signals of two detectors placed at the positions of equivalent speckles are correlated. However, the correlation is not perfect: On the

one hand both detectors also ''see'' light from the other scattering experiment, on the other hand, they detect multiply scattered light of the two incoming laser beams. The multiply scattered light, however, is totally uncorrelated. These two contributions to the detector signal do not contribute to the time dependent signal of the correlated intensities but only to an enhanced background.

As mentioned above each of both detectors receives scattered light from both illuminating laser beams. Therefore we denote by $\mathbf{E}_{A1}(t)$ and $\mathbf{E}_{A2}(t)$ the field amplitudes of the scattered light components detected by detector A and resulting from the illuminating light beams 1 and 2, respectively. Then, the entire field amplitude $\mathbf{E}_A(t)$ can be decomposed as

$$\mathbf{E}_A(t)=\mathbf{E}^s_{A1}(t)+\mathbf{E}^m_{A1}(t)+\mathbf{E}^s_{A2}(t)+\mathbf{E}^m_{A2}(t), \tag{2.1}$$

where the superscripts s and m stand for *singly* and *multiply* scattered light, respectively. The corresponding expression for $E_B(t)$ is obtained by replacing A and B in Eq. (2.1).

Considering the correlations between these field amplitudes, one finds that only the correlations between E^s_{A1} and E^s_{B2} do not vanish: The multiply scattered contributions E^m_{A1}, E^m_{A2}, E^m_{B1}, and E^m_{B2} have different intermediate scattering vectors and are therefore uncorrelated. Furthermore, it can be shown that if the angle ϕ between the laser beams 1 and 2 complies with the relation $\mathbf{\Delta q}=|\mathbf{q}_{A2}-\mathbf{q}_{B1}|>|2\pi/d|$, where d denotes the diameter of the scattering volume in direction of the vector $\mathbf{\Delta q}$, the correlations between $E^s_{A2}(t)$ and $E^s_{B1}(t)$ can be neglected [23,24], too.

In general, the *normalized cross correlation function* $C(7\tau,\theta)$ of scattering angle θ is given by

$$C(\tau,\theta)=\frac{\langle I_A(0,\theta)I_B(\tau,\theta)\rangle}{\langle I_A(\tau,\theta)\rangle\langle I_B(\tau,\theta)\rangle}, \tag{2.2}$$

with the lag time τ and the intensity $I_A(t)=|E_A(t)E^*_A(t)|$. The brackets ''$\langle\ \rangle$'' denote a time average, which for ergodic processes is equal to the ensemble average. With above assumptions the normalized 3D cross correlation function $C(\tau,\theta)$ is related to the well investigated normalized field correlation function $G(\tau,\theta)$ of singly scattered light [20]:

$$C(\tau,\theta)=\frac{\langle I^s_{A1}(\theta)\rangle\langle I^s_{B2}(\theta)\rangle}{\langle I_A(\theta)\rangle\langle I_B(\theta)\rangle}\beta_\theta|G(\tau,\theta)|^2+1. \tag{2.3}$$

β_θ denotes a prefactor that considers the reduction of the amplitude by misalignment effects and the finite detector size. β_θ can be determined experimentally by measurement of the amplitude for nearly transparent samples with concentration $c\to 0$ where $\langle I_A(\theta)\rangle=\langle I^s_A(\theta)\rangle$.

By Eq. (2.3), the direct problem of the 3D cross correlation method is reduced to the common direct problem of DLS, which has to be modified for the multiangle analysis as described in the following section.

III. DIRECT PROBLEM AND OBSERVATION EQUATION

For an ideal light scattering experiment the relation between the normalized field correlation function and the relaxation time spectrum is given by

$$G(\tau,\theta)=\int_{-\infty}^{\infty} d\ln\alpha\,\tilde{h}_\alpha(\alpha,\theta)e^{-\tau/\alpha}. \tag{3.1}$$

The relaxation time spectrum $\tilde{h}_\alpha(\alpha,\theta)$ describes (in dependence on the scattering angle θ) the relative scattering contribution of a particle with relaxation time α to the normalized field correlation function. For spherical particles the relaxation time α can be related to the *hydrodynamic radius* r_h using the Einstein-Stokes relation [25]

$$\alpha=\frac{6\pi\eta}{\mathbf{q}^2(\theta)k_BT}r_h=:\frac{1}{c(\theta)}r_h, \tag{3.2}$$

where η is the viscosity and T the temperature of the fluid, and k_B denotes the Boltzmann constant. Introducing the angle dependent parameter $c(\theta)$ in Eq. (3.2) and substituting the relaxation time α by the hydrodynamic radius r_h the cross correlation function now reads according to Eq. (2.3)

$$C(\tau,\theta)=a_\theta\left[\int_{-\infty}^{\infty} d\ln r_h\tilde{h}_r(r_h,\theta)e^{-c(\theta)\tau/r_h}\right]^2+1, \tag{3.3}$$

with $\tilde{h}_r(r_h,\theta)$ being the relative scattering contribution of a particle with radius r_h, which again depends on the scattering angle. The prefactor a_θ is given by

$$a_\theta=\frac{\langle I^s_{A1}(\theta)\rangle\langle I^s_{B2}(\theta)\rangle}{\langle I_A(\theta)\rangle\langle I_B(\theta)\rangle}\beta_\theta. \tag{3.4}$$

In the next step the angle dependence of the distribution $\tilde{h}_r$ is ''removed,'' i.e., the relative scattering contribution is substituted by the *radius distribution* h_r that is, of course, independent of the scattering angle. The angle dependence of the relative scattering contribution $\tilde{h}_r(r_h,\theta)$ is evoked by the scattering characteristic of the particles which is described for spherical particles by the Mie coefficients $f_{\mathrm{Mie}}(r_h,\theta)$. The scattering characteristic can be calculated for other types of particles, but their shape have to be uniform and known beforehand.[1] In the following spherical particles are assumed.

Introducing the Mie coefficients and the angle independent radius distribution $h_r(r_h)$ into Eq. (3.3) the direct problem now reads

[1]Note that Eq. (3.2) has to be modified for nonspherical particles, too.

$$C(\tau,\theta)=a_\theta\left[\int_{-\infty}^{\infty} d\ln r_h h_r(r_h) f_{\mathrm{Mie}}(r_h,\theta) e^{-c(\theta)\tau/r_h}\right]^2+1, \tag{3.5}$$

so that one can describe *all* data of all scattering angles by *one* distribution $h_r(r_h)$.

Sometimes, however, it is favorable or even necessary to estimate the relative scattering contribution $\tilde{h}(r_h,\theta_{\mathrm{ref}})$ with regard to a reference angle θ_{ref} [8]. Then the direct problem can be written as

$$C(\tau,\theta)=a_\theta\left[\int_{-\infty}^{\infty} d\ln r_h \tilde{h}_r^{\theta_{\mathrm{ref}}}(r_h)\frac{f_{\mathrm{Mie}}(r_h,\theta)}{f_{\mathrm{Mie}}(r_h,\theta_{\mathrm{ref}})} e^{-c(\theta)\,\tau/r_h}\right]^2 +1 \tag{3.6}$$

and for $\theta\to\theta_{\mathrm{ref}}$ Eq. (3.6) becomes equal to Eq. (3.3). Thus, one again can describe the data of *all* scattering angles by *one* distribution $\tilde{h}_r^{\theta_{\mathrm{ref}}}(r_h)$.

Empirically, the estimation of distributions in such direct problems depends sensitively on aberrations in the baseline of the data. Furthermore, not even all hardware correlators are able to estimate the *normalized* correlation function. Therefore, in the following the more general case of a non-normalized correlation function is considered and the baselines of the correlation functions, denoted with b_θ, for each measurement angle θ_l are estimated simultaneously, too. Thus, Eq. (3.5) and (3.6) read

$$C(\tau,\theta)[h_r,a_\theta,b_\theta] = a_\theta\left[\int_{-\infty}^{\infty} d\ln r_h h_r(r_h) f_{\mathrm{Mie}}(r_h,\theta) e^{-c(\theta)\tau/r_h}\right]^2+b_\theta, \tag{3.7}$$

$$C(\tau,\theta)[\tilde{h}_r^{\theta_{\mathrm{ref}}},a_\theta,b_\theta] = a_\theta\left[\int_{-\infty}^{\infty} d\ln r_h \tilde{h}_r^{\theta_{\mathrm{ref}}}(r_h)\frac{f_{\mathrm{Mie}}(r_h,\theta)}{f_{\mathrm{Mie}}(r_h,\theta_{\mathrm{ref}})} e^{-c(\theta)\tau/r_h}\right]^2 +b_\theta. \tag{3.8}$$

Here, the squared brackets indicate that Eqs. (3.7) and (3.8) can be interpreted as functionals of the parameters a_θ, b_θ and the distribution h_r or $\tilde{h}_r^{\theta_{\mathrm{ref}}}$, respectively. These relations between the data and the distribution represent the so-called *direct problem* that has to be inverted in order to obtain a_θ, b_θ and h_r or $\tilde{h}_r^{\theta_{\mathrm{ref}}}$, respectively.

The *measured correlation function* $C^\sigma(\tau,\theta)$ can be assumed as a realization of a Gaussian random variable with mean $C(\tau,\theta)$:

$$C^\sigma(\tau_i,\theta_l)=C(\tau_i,\theta_l)+e(\tau_i,\theta_l), \tag{3.9}$$

where the *data errors* $e(\tau_i,\theta_l)$ are a realization of a random variable $E(\tau_i,\theta_l)$ with

$$\langle E(\tau_i,\theta_l)\rangle=0, \tag{3.10}$$

$$\mathrm{Var}[E(\tau_i,\theta_l)]=\sigma_i^2(\theta). \tag{3.11}$$

Eq. (3.9) represents the so-called *observation equation*.

The assumption of Gaussian distributed errors is due to the fact that the correlation function $C(\tau_i,\theta_l)$ sums up the photon numbers that itself can be regarded as realizations of random variables with bounded variance. Thus, according to the *law of large numbers*, the distribution of the random variable $C^\sigma(\tau_i,\theta_l)$ converges to a Gaussian distribution.

IV. REGULARIZATION METHOD

In Sec. II the cross correlation function of 3D cross correlation measurements has been related to the well investigated normalized field correlation function and thus to the common direct problem of DLS. Then, in Sec. III this direct problem has been modified by introducing the scattering characteristic of the solved particles, so that the data of all measurement angles can be described by *one* distribution h_r or $\tilde{h}_r^{\theta_{\mathrm{ref}}}$, respectively. In the following, regularization methods are adapted to the results of Sec. III to obtain a multi-angle estimator for the radius distribution.

Commonly, the regularization solution is obtained by minimizing the following functional:

$$V_\lambda[h]=\sum_{i=1}^{N}\frac{1}{\sigma_i}(C_i^\sigma-C_i[h])^2+\lambda R[h], \tag{4.1}$$

where N is the number of data points and σ_i is the standard deviation of the measurement error of the data point C_i^σ.

For a given data model (i.e., direct problem) expressed by $C[h]$, the sum in Eq. (4.1) determines the *discrepancy* of the measured data C^σ from the corresponding value $C[h]$ under the hypothesis that h is the true distribution. The smaller the discrepancy, the better h fits the data on the basis of the model. Thus the regularization solution is forced to be compatible with the data. The minimization of this term alone corresponds to ordinary (non negative) least square estimations.

The *regularization term* $R[h]$ imposes the constraint from some prior information by assigning to h a value that is the smaller the better h complies with the prior information, i.e., the more probable it is considered. Note that the prior information is independent from the data.

The *regularization parameter* λ weights the constraint from the prior information in comparison with the constraint from the data. For a proper estimation of h an optimal value of λ has to be chosen. This optimal value highly depends on the measurement errors and the number of data points. In this article λ is selected by means of the self-consistent method introduced by Honerkamp and Weese [4].

Minimization of the functional $V_\lambda[h]$ in Eq. (4.1) in order to obtain an estimate of the distribution h corresponds to a MAP estimator (see, e.g., [6,26]). With Eq. (3.7) or Eq. (3.8), respectively, and Eq. (4.1) the multiangle MAP estimator of the radius distribution h_r and the parameters a_{θ_l} and b_{θ_l} reads

$$\{\hat{h}_r^{\mathrm{ma}},\hat{a}_{\theta_l},\hat{b}_{\theta_l}\}=\arg\min_{h_r,a_{\theta_l},b_{\theta_l}}\left\{\sum_{l=1}^{L}\sum_{i=1}^{N_l}\frac{\{C^{\sigma}(\tau_i,\theta_l)-C[h_r,a_{\theta_l},b_{\theta_l}](\tau_i,\theta_l)\}^2}{\sigma_i^2}+\lambda R[h_r]\right\}. \tag{4.2}$$

Here, L denotes the number of measurement angles and N_l is the number of data points of the correlation function $C^{\sigma}(\tau_i,\theta_l)$ obtained at angle θ_l.

Analogously, for the single angle MAP estimator it follows that

$$\{\hat{h}_r^{\mathrm{sa}},\hat{a}_{\theta},\hat{b}_{\theta}\}=\arg\min_{h_r,a_{\theta},b_{\theta}}\left\{\sum_{i=1}^{N_{\theta}}\frac{\{C^{\sigma}(\tau_i,\theta)-C[h_r,a_{\theta},b_{\theta}](\tau_i,\theta)\}^2}{\sigma_i^2}+\lambda R[h_r]\right\}. \tag{4.3}$$

In the case of radius distributions one prior information is the positivity constraint $h_r(r)\geqslant 0\forall r$. The positivity constraint is enforced by the minimization algorithm, which allows only positive values for the distribution. Furthermore, one can assume, that the distribution is *limited*. This prior information is modeled by the so-called *Tikhonov regularization term*

$$R[h_r]=\sum_{l=1}^{M}h_r^2(r_i). \tag{4.4}$$

This functional has been used for the estimation of the monomodal radius distribution h_r in Sec. VI.

For broadened distributions the prior information that the distribution is *smooth* may be more appropriate. This smoothness constraint is modeled by the *Phillips regularization term*

$$R[h_r]=\sum_{i=2}^{M-1}[h_r(r_{i+1})-2h_r(r_i)+h_r(r_{i-1})], \tag{4.5}$$

which sums up the numerical approximation of the second derivatives of the distribution. This functional has been used for the estimation of the bimodal relative scattering contribution $\tilde{h}_r^{50^\circ}$ in the second part of Sec. VI.

As mentioned above, regularization methods can be interpreted in the framework of Bayesian estimators as MAP estimators. From this point of view the minimization of the functional $V_\lambda[h]$ corresponds to the maximization of the *a posteriori* distribution $\rho(h|C^{\sigma})$, which represents the most probable distribution h given the data C^{σ}. For a more detailed discussion we refer to [6,26].

V. EXPERIMENT

All measurements have been performed using an optimized 3D cross correlation instrument. As demonstrated in [21,20,27] this measurement scheme avoids any deterioration of the measured correlation function by multiply scattered light and allows the investigation of samples up to fairly high turbidity levels. The radii of the latex particles obtained by TEM measurements provided by the manufacturer (Dow) are 226.5 ± 4.5 nm, 66.0 nm (no standard deviation given by the manufacturer), and 53.5 ± 5.25 nm. The investigated samples contain latex particles with a refractive index of $n=1.59$ and a density of $\rho=1.05$ g/ml. For all measurements the temperature was kept at 20.6 ± 0.2°C. In the following we consider two different types of sample: an aqueous suspension of latex particles with a fairly narrow size distribution and a bimodal sample containing latex spheres of two distinct sizes.

a. Monomodal sample. Figure 2 shows the cross correlation functions of the scattered intensity for the monomodal sample (τ axis with logarithmic scale) for different scattering angles. The radius of the latex particles obtained by TEM

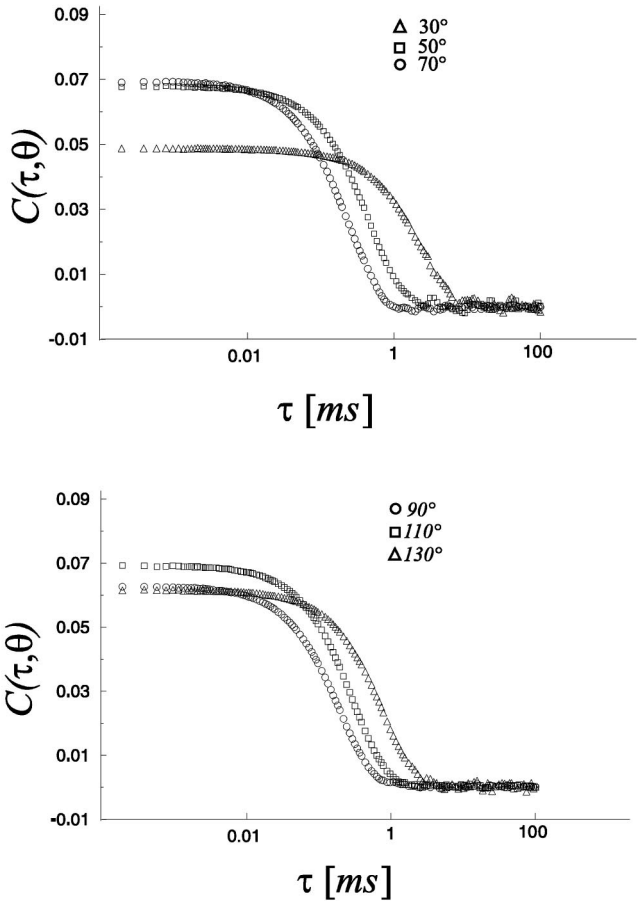

FIG. 2. Cross correlation functions obtained for a monomodal suspension. TEM radius of the suspended latex particle is 53.5 $\pm$5.25 nm. The scattering angle θ_l ranges from 30° to 130° in steps of 20°.

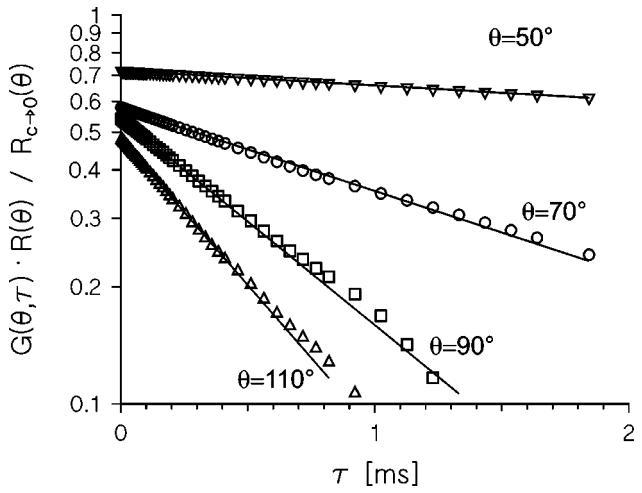

FIG. 3. 3D cross correlation functions obtained for a bimodal suspension. The TEM radii of the suspended latex particles have been 226.5 and 66.0 nm. The cross correlation functions have been measured in an angular range of $50° \leqslant \theta \leqslant 110°$ at intervals of 20°, the turbidity has been 2.60 cm^{-1}. For clarity of presentation the data of the auto correlation functions for $\theta = 50°, 70°$, and 90° have been given an offset.

measurements provided by the manufacturer is 53.5 ± 5.25 nm. The range of the measurement angles has been chosen from 30° to 130° in steps of 20°. The mass ratio of latex to solvent is 0.3%. Accordingly, the sample is indeed quite turbid. The turbidity τ of the samples was obtained using the relation $\tau = \ln(I_0/I_{\text{trans}})/l$, where I_{trans} is the intensity of the transmitted laser light in the presence of the sample, I_o is the corresponding value for the cell filled with pure water and $l = 10$ mm is the thickness of the sample. With $\tau = 3.08$ cm^{-1} the monomodal sample was rather turbid.

Obviously, the errors of the cross correlation functions increase for long relaxation times, which complicates a proper estimation of the baseline. Furthermore, this behavior of the errors stands in contradiction to the error model for autocorrelation functions proposed by Schätzel [28] that predicts substantially an exponential decay of the estimation errors for long relaxation times. Accordingly, this error model is *ad hoc* not transferable to the case of cross correlation functions and in the following a simple but more adequate error model with absolute errors is assumed.

b. Bimodal sample. Next we performed measurements with a strongly scattering bimodal sample containing particles with radii of 226.5 ± 4.5 nm and 66.0 nm (no standard deviation available), obtained by TEM measurements provided by the manufacturer. The ratio of the mass concentration c_1/c_2 of the particles is 1:20.2. The turbidity of the sample was $\tau = 2.60$ cm^{-1}. Figure 3 shows 3D cross correlation functions of the electric field amplitude for several scattering angles (G axis with logarithmic scale).

The time dependence of the measured 3D cross correlation functions—which takes only single scattering processes into account—does not show observable deviations from a simple exponential (indicated by the solid line). Despite this simple exponential behavior the sample is bimodal, however. The appearance of just *one* single exponential is due to the relatively small size ratio of 1:3.4 where the two contributions result in a cross correlation function that appears to be monoexponential (but actually *is* bimodal). This example demonstrates, that in many cases it is difficult or even impossible to yield reliable information about the constituents by measurements from a *single* scattering angle only.

VI. EVALUATION

In the following section the radii distribution h_r calculated for the monomodal sample and the relative scattering contribution $\tilde{h}_r^{\theta_{\text{ref}}}$ of the bimodal sample are estimated with both the *single angle* and the *multiangle* MAP estimator. Furthermore, for the bimodal sample the volume fraction of the two components is calculated from the relative scattering contribution estimated by the maMAP estimator. Then, this volume fraction is compared to the experimentally determined volume fraction. It is shown that the multiangle analysis enhances enormously the resolution of the estimation. Moreover, the calculated volume fraction agrees qualitatively with the ''real'' volume fraction—despite the low signal-to-noise ratio.

a. Monomodal sample. First we consider the results obtained for the monomodal sample. Here, the simultaneous analysis of cross correlation functions for only three different scattering angles is sufficient to enhance the quality of the reconstructed radius distribution enormously. In order to demonstrate that this result is consistent and quite independent of the choice of the measurement angles the radius distribution is estimated for two different sets of three cross correlation functions. These sets consist of the cross correlation functions measured at 30°,70°,110° and 50°,90°,130°, respectively.

The shape of the radius distribution is shown in Fig. 4. The estimates of the radius distribution (error bars) were calculated with the saMAP estimator. Each single angle estimation leads to strongly broadened and asymmetric radius distributions in contrast to the TEM measurements. Moreover, the estimation of the radius distribution of the measurement angle $\theta = 110°$ is even bimodal. Obviously, the shape of the radius distribution cannot be reconstructed from these noisy data using the saMAP estimator.

Figure 5 shows the estimates of the radius distribution obtained with the maMAP estimator: Unlike the saMAP estimator the maMAP estimator is able to reconstruct properly the shape of the radius distribution: the estimates are narrow distributions with mean 50 nm and a standard deviation of 2.2 nm.

We now turn to a rather important subject that in practical applications is astonishingly often neglected. This is the comparison of the position of the maximum values of r_{max} with the mean radii r_{mean}. For single angle estimates (cf. Table I) the maxima vary from 46 nm up to 53 nm. Furthermore, the asymmetric shape of the distribution has an impact on the mean radii, which differs significantly from the position of the maximum radii and also from the ''real'' radius measured by TEM. This means, in such cases it is difficult to make a clear prediction about particle size and distribution shape.

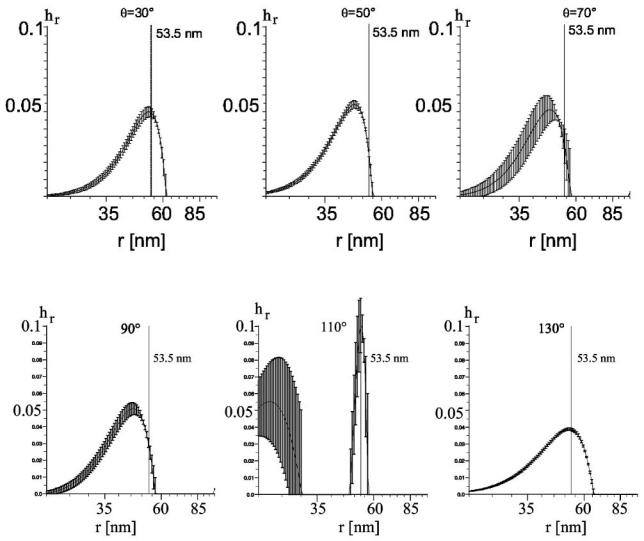

FIG. 4. Estimates (error bars) of a monomodal radius distribution using the saMAP estimator. The radius size obtained from TEM measurements provided by the manufacturer is $r=53{,}5\pm5.25$ nm (indicated by the solid line). For each measurement angle a broadened radius distribution is calculated. In particular, the width of the distributions are far larger than the width of the original distribution. The maxima and mean radii of the distributions vary strongly for all measurement angles as shown in Table I.

In contrast to that, evaluation of the 3D cross correlation function by the maMAP estimator give reliable results: now, the maximum value of the size distribution for each *set* of scattering angles yields the same value 50 nm. Furthermore, this result is consistent with the results of the mean radius of 50 nm for each set. To conclude, we state that the *particle size* as well as the *distribution shape* are properly estimated by the maMAP estimator (cf. Fig. 5).

b. Bimodal sample. In this section we consider the evaluation of the bimodal sample. Here, the volume fractions of the two components are very different (1:20.2). Thus, an estimation of the radius distribution might lead to an smoothing of the smaller component (large particles), although the data contain sufficient information about this component due to the strong increase of the scattering characteristic for the

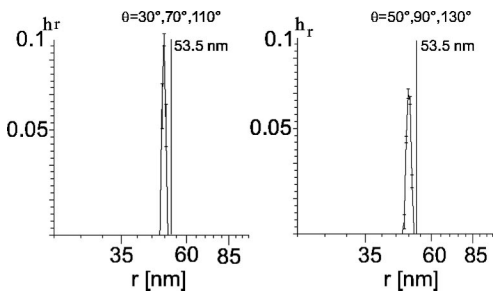

FIG. 5. Estimates (error bars) of a monomodal radius distribution using the maMAP estimator. The radius size obtained from TEM measurements provided by the manufacturer is $r=53{,}5\pm5.25$ nm (indicated by the solid line). Both estimations lead to the same consistent maximum at 50 nm. Furthermore the shape of the distribution is very close to the TEM measurements.

TABLE I. Monomodal distribution: Estimated maximum and mean radius in nanometers.

Radius (TEM): 53.0					
saMAP			maMAP		
θ	r_{max} (nm)	r_{mean} (nm)	θ	r_{max} (nm)	r_{mean} (nm)
30°	52	48	30°, 70°, 110°	50	50
50°	47	42	50°, 90°, 130°	50	50
70°	47	43			
90°	46	43			
110°	(22)[a], 53 (39)[b],	51			
130°	52	48			

[a]First peak of the bimodal reconstruction.
[b]Taking both peaks into consideration.

larger particles. However, this problem can be overcome by estimation of the relative scattering contribution $\tilde{h}_r^{\theta_{ref}}$ instead of h_r [cf. Eqs. (3.7) and (3.8)] as described in Sec. III. Figure 6 shows the estimates of the relative scattering contribution $\tilde{h}_r^{50°}$ for the reference angle $\theta_{ref}=50°$, calculated by the saMAP estimator. Again, the saMAP estimator is not able to reconstruct properly the shape of the radius distribution. In particular, it cannot resolve the bimodal character of the distribution. The relative scattering contributions estimated from cross correlation functions of the measurement angles 50°, 70°, and 110° show contributions of the large particle component, indicated by an increase of the distribution for large particle sizes (50°,70°), or by a broadening of the dis-

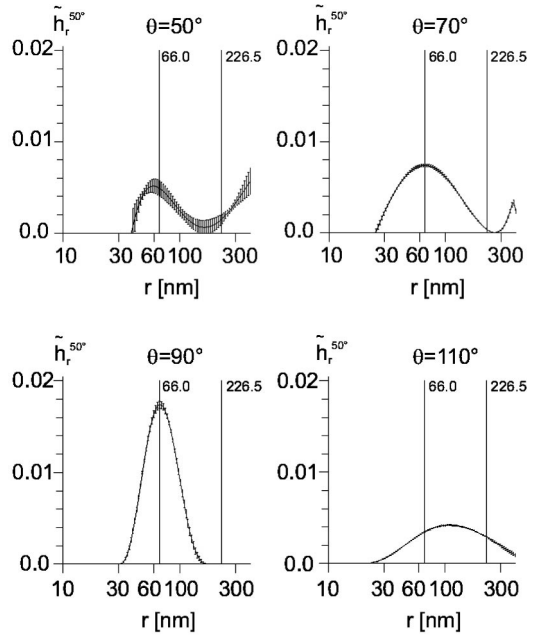

FIG. 6. Single angle estimates (error bars) of a bimodal relative scattering contribution $\tilde{h}_r^{50°}$ to the reference angle $\theta_{ref}=50°$. The radii sizes obtained from TEM measurements provided by the manufacturer are $r_1=66.0$ nm and $r_2=226.5$ nm (indicated by the solid lines). The saMAP estimator is not able to reconstruct the bimodal character of the radius distribution.

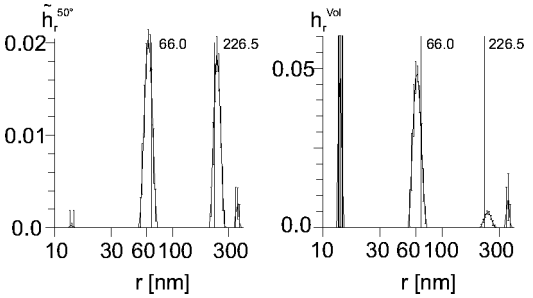

FIG. 7. Left: Multiangle estimate (error bars) of a bimodal relative scattering contribution $\tilde{h}_r^{50°}$ for the reference angle $\theta_{\mathrm{ref}}=50°$. The radii sizes obtained from TEM measurements provided by the manufacturer are $r_1=66.0$ nm and $r_2=226.5$ nm (indicated by the solid lines). The multiangle estimator reconstructs properly both components of the bimodal distribution. The small peaks at $r=14$ nm and at $r=357$ nm are affected with large errors and are not significant. Accordingly, they can be neglected in comparison with the main peaks. Right: Volume fraction calculated from the relative scattering contribution $\tilde{h}_r^{50°}$ rendering a mass concentration of 10.3:1.

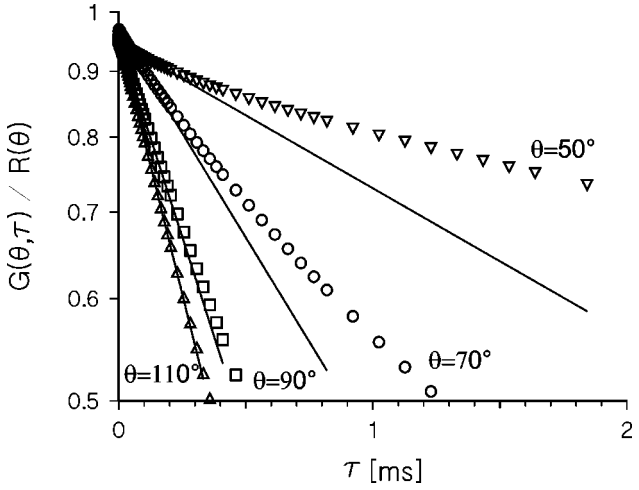

FIG. 8. Conventional auto correlation functions obtained for a bimodal suspension. The TEM radii of the suspended latex particles have been 226.5 and 66.0 nm. The auto correlation functions have been measured in an angular range of $50°\leqslant\theta\leqslant 110°$ at intervals of 20°, the turbidity has been 2.60 cm^{-1}. For clarity of presentation the data of the auto correlation functions for $\theta=50°,70°$, and 90° have been given an offset.

tribution (110°). This is due to the fact that larger particles have a scattering minimum between $\theta=80°$ and $\theta=90°$. Therefore the result at $\theta=90°$ results mostly from light scattered by the smaller particles. Consequently, the time dependence of the cross correlation functions at this scattering angle mostly reflects the dynamic of smaller particles and the contribution of the particles with radius $r=226.5$ nm is negligible.

The maMAP estimate of the relative scattering contribution $\tilde{h}_r^{50°}$ (Fig. 7), however, resolves both components at $r_1^{\mathrm{maMAP}}=62$ nm and $r_2^{\mathrm{maMAP}}=237$ nm in good agreement with the TEM measurements (indicated by the solid lines). The two small peaks at $r=14$ nm and at $r=357$ nm are affected with large estimation errors and are not significant since they are compatible with zero. On the right hand side of Fig. 7 the volume fraction calculated from the relative scattering contribution $\tilde{h}_r^{50°}$ is shown. The calculated volume fraction of 10.3:1 differs from the ''real'' volume fraction of 20.2:1 by a factor of 2. This is probably due to the low signal-to-noise ratio of the experimental data.

VII. SUMMARY AND DISCUSSION

In this paper we have demonstrated that the combination of modern measurement methods and enhanced data analysis enables to analyze ''real world'' systems, even for high turbidity levels. Especially when the signal-to-noise ratio of the experimentally obtained data is low, e.g., in the case of 3D cross correlation measurements of turbid media, the multiangle analysis combined with the simultaneous regularization method (maMAP estimator) enhances enormously the quality of the evaluation results.

For the investigation of turbid media it is essential to apply measurement methods that select only that part of the scattered light that stems from single scattering processes. This is especially important for bimodal samples, where the effect of multiple scattering can be mistaken as if caused by a broad size distribution. This is demonstrated in Fig. 8 that shows autocorrelation functions of the electric field amplitude obtained with a conventional DLS experiment for the same sample as in Fig. 3. As can be inferred from Fig. 8 the measured autocorrelation functions differ significantly from a monoexponential decay (indicated by solid line), especially for small scattering angles. This could easily lead to misinterpretations of the data: These deviations could be interpreted as if they were caused by a broad or multimodal distribution of particle sizes. However, in this case the observed deviations do not result from different contributions of scattering particles but from the influence of multiple scattering. This is confirmed by the 3D cross correlation functions in Fig. 3 that result only from single scattering processes and are not affected by the disturbing influence of multiple scattering.

Furthermore, the 3D cross correlation functions of the bimodal sample also show that it is often not possible to yield reliable results from measurements at only one scattering angle. The correlation functions of Fig. 3 appear to be a single exponential as expected for samples containing only one type of scatterer, despite the fact that the sample contains scatterer of two distinct sizes. In such cases, only evaluation schemes on the basis of multiangle procedures lead to the desired information about the constituents of the sample. This has been shown in [29] in a straight forward way, where a simple fit procedure has been presented that is based on the simultaneous evaluation of dynamic and static light scattering data. It has been shown that this procedure leads to reliable results concerning the composition of the bimodal samples under investigation, even for samples where the size of the scattering particles differ only by a factor of 1.9. The clear advantage of this simple fit procedure is its easy handling: one only needs to determine the initial slope of the

correlation functions, which in general can easily be done, even for correlation functions with low signal-to-noise ratio. This of course means, that this simple procedure is not able to determine the *shape* of the particle size distribution.

In contrast to that, we have demonstrated that the maMAP estimator is able to reconstruct properly both the position and the shape of bimodal particle size distributions—in contrast to evaluations of the saMAP estimator for just one scattering angle. The improved resolution of the multiangle estimator compared to the single angle estimator is due to a number of reasons.

(1) The resolution of a single angle estimator varies for specific particle sizes in dependence of the measurement angle. This is caused by the fact that—in dependence on the scattering angle—specific particle sizes contribute less to the entire scattering intensity and thus to the entire correlation function. The multiangle estimator, however, compensates the lower information on specific particle sizes at *one* measurement angle by information of *the other* measurement angles. Thus the resolution of the multiangle estimator is quite equal for all particle sizes.

(2) Furthermore, for every particle size the resolution of the multiangle estimator is better than the resolution of the ''best'' single angle estimator, which is due to a larger number of data.

(3) At last, in the case of the maMAP estimator the prior information is imposed to *one* consistent solution on basis of *all* measured data, whereas in the case of the saMAP estimator the prior information is imposed to each single angle solution separately. Thus the combination of all single angle solutions is not the best solution with respect to the prior information and all data [6].

Concluding, one can state that the simultaneous regularization method discussed in this paper is a powerful tool in order to reconstruct the radius distribution or relative scattering contribution, respectively—especially from data with a low signal-to-noise ratio as in the case of turbid media or highly diluted samples when single angle regularization methods fail in resolving the distribution. In some publications [28,30] more elaborated error models have been proposed, where the correlations of errors have to be taken into consideration. In particular, it has been shown that in case of high intensities and short measurement times the correlations of the errors should not be neglected [7,31]. However, an improved error model for the present 3D cross correlation data has—according to our knowledge—not been proposed up to now and the transferability of Schätzels error model to cross correlation data is still not proved. Also in this paper we focus on the *multiangle* data analysis, so that we restrict ourselves to the simplified error model.

Finally, if the distribution cannot be reconstructed properly using the simplified error model, one should investigate the data using an improved error model. However, if the distribution is reconstructed well with the simplified error model an improved error model will not enhance significantly the resolution [31]. As shown below for the data used in this paper the results of the MAP estimator are quite good so that one cannot expect improving results by taking account of an improved error model.

[1] A. K. Louis, *Inverse und Schlecht Gestellte Probleme* (Teubner, Stuttgart, 1977).

[2] V. A. Morozov, *Methods for Solving Incorrectly Posed Problems* (Springer, Berlin, 1984).

[3] C. W. Groetsch, *The Theory of Tikhonov Regularization for Fredholm Equations of the First Kind* (Pitman, London, 1984).

[4] J. Honerkamp and J. Weese, Continuum Mech. Thermodyn. **2**, 17 (1990).

[5] J. Honerkamp, D. Maier, and J. Weese, J. Chem. Phys. **98**, 865 (1993).

[6] R. Buttgereit, M. Marth, T. Roths, and J. Honerkamp, Macromol. Symp. **162**, 149 (2000).

[7] R. Buttgereit, M. Marth, and J. Honerkamp, Macromol. Symp. **162**, 173 (2000).

[8] C. de Vos, L. Deriemaeker, and R. Finsy, Langmuir **12**, 2630 (1996).

[9] G. Bryant and J. C. Thomas, Langmuir **11**, 2480 (1995).

[10] G. Bryant, C. Abeynayake, and J. C. Thomas, Langmuir **11**, 2480 (1995).

[11] P. N. Segre, W. van Mengen, P. N. Pusey, K. Schätzel, and W. Peters, J. Mod. Opt. **42**, 1929 (1995).

[12] G. D. J. Phillies, Phys. Rev. A **24**, 1939 (1981).

[13] H. J. Mos, C. Pathmamanoharan, J. K. G. Dhont, and C. G. de Kruif, J. Chem. Phys. **84**, 45 (1986).

[14] M. Drewel, J. Ahrens, and U. Podschus, J. Opt. Soc. Am. A **7**, 206 (1990).

[15] C. Urban and P. Schurtenberger, Prog. Colloid Polym. Sci. **110**, 61 (1997).

[16] W. V. Meyer, D. S. Cannell, A. E. Smart, T. W. Taylor, and P. Tin, Appl. Opt. **36**, 7551 (1997).

[17] K. Schätzel, J. Mod. Opt. **38**, 1849 (1991).

[18] C. Urban and P. Schurtenberger, Phys. Chem. Chem. Phys. **1**, 3911 (1999).

[19] L. B. Aberle, S. Wiegand, W. Schröer, and W. Staude, Prog. Colloid Polym. Sci. **104**, 121 (1997).

[20] L. B. Aberle, P. Hülstede, S. Wiegand, W. Schröer, and W. Staude, Appl. Opt. **37**, 6511 (1998).

[21] L. B. Aberle, M. Kleemeier, P. Hülstede, S. Wiegand, W. Schröer, and W. Staude, J. Phys. D **32**, 22 (1999).

[22] C. Wu, K. Unterforsthuber, D. Lilge, E. Lüddecke, and D. Horn, Part. Part. Syst. Charact. **11**, 145 (1994).

[23] B. J. Berne and R. Pecora, *Dynamic Light Scattering* (Wiley, New York, 1976).

[24] L. B. Aberle, Ph.D. thesis, Universität-Gesamthochschule Siegen, 1999.

[25] G. Strobl, *The Physics of Polymers* (Springer-Verlag, Berlin, 1997).

[26] J. Honerkamp, *Statistical Physics* (Springer, Berlin, 1998).

[27] L. B. Aberle, W. Staude, and O.-D. Hennemann, Phys. Chem. Chem. Phys. **1**, 3917 (1999).

[28] K. Schätzel, Quantum Opt. **2**, 287 (1990).
[29] L. B. Aberle, P. Hülstede, M. Kleemeier, W. Staude, and O.-D. Hennemann, Macromol. Symp. **162**, 249 (2000); **162**, 269 (2000).
[30] K. Schätzel and R. Peters, Photon Correlation Spectroscopy Multicomponent System **1430**, 109 (1991).
[31] D. Maier, M. Marth, J. Weese, and J. Honerkamp, Appl. Opt. **38**, 4671 (1999).